*Article citation info:*
Ajiban MH, Sudarmanta B. Synergistic effects of hydrogen enrichment and EGR on the performance and emissions of a diesel dual fuel engine: a statistical investigation. Combustion Engines. 0000;XXX(X):xx-xx. https://doi.org/10.19206/CE-220595

*Mochammad Hildad AJIBAN*
*Bambang SUDARMANTA*

Combustion Engines
Polish Scientific Society of Combustion Engines

# Synergistic effects of hydrogen enrichment and EGR on the performance and emissions of a diesel dual fuel engine: a statistical investigation

ARTICLE INFO

Received: 27 December 2025
Revised: 29 March 2026
Accepted: 12 April 2026
Available online: 24 April 2026

*Balancing the demand for high thermal efficiency with strict $NO_x$ emission limits remains a persistent dilemma in modern diesel engine development. This study explores a potential solution by investigating how hydrogen enrichment interacts with EGR in a diesel dual-fuel engine under constant load. Instead of treating these variables in isolation, we employed a randomized full factorial design to map their simultaneous effects, testing hydrogen flow rates up to 7.5 LPM and EGR levels up to 15%. Through rigorous statistical analysis (ANOVA and Tukey's HSD), we uncovered a distinct "sweet spot" in engine operation. While hydrogen injection successfully boosted thermal efficiency and reduced fuel consumption due to its rapid combustion, it was expected to trigger a spike in $NO_x$ emissions. However, our analysis revealed a crucial interaction: adding 10% EGR effectively neutralized this emission penalty without severely crippling the engine power. Interestingly, we also identified a saturation point at 7.5 LPM of hydrogen, beyond which the engine ceased to improve in efficiency due to volumetric losses. Ultimately, the data suggests that pairing 5.0 LPM of hydrogen with 10% EGR offers the most balanced configuration restoring power to baseline levels while keeping emissions in check.*

Key words: *ANOVA, biodiesel, diesel dual-fuel, hydrogen-EGR interaction, $NO_x$ trade-off*



## 1. Introduction

The global energy crisis and environmental degradation caused by fossil fuel combustion have become key catalysts in the fundamental transformation of the transportation and power generation sectors [12]. At the national level, Indonesia commitment to achieving NZE by 2060 has been outlined in a strategic roadmap that prioritizes the energy transition [10]. CI engines remain the cornerstone in industrial and heavy transportation sectors due to their high thermal efficiency, robust durability, and superior fuel economy [33]. However, the sustainability of CI engine use is increasingly threatened by stricter emissions regulations, such as the Euro 6 standards and national decarbonization targets that mandate progressive reductions in greenhouse gas emissions [5].

Although CI engines offer high efficiency, their application faces complex environmental challenges [7]. In general, diesel dual fuel engines are recognized as major contributors to $NO_x$ and PM/soot emissions, stemming from their inherent combustion trade-offs [24]. Yet, emission issues are not limited to these two pollutants. Byproducts of incomplete combustion, such as CO and HC, along with $CO_2$ greenhouse gas emissions, pose significant concerns [6]. The accumulation of these emissions not only presents serious carcinogenic risks to human health but also significantly contributes to global warming, thereby underscoring the urgent need for comprehensive mitigation strategies [2].

One of the most promising approaches to address these challenges is the use of renewable alternative fuels, such as biodiesel. However, biodiesel utilization is often constrained by its lower calorific value compared to pure diesel combustion, which negatively impacts engine performance [25]. To compensate for this limitation, dual-fuel technology with hydrogen ($H_2$) supplementation has gained considerable attention as a future energy solution [30]. Nationally, hydrogen development has been designated as a key pillar in Indonesia Hydrogen and Ammonia Roadmap, where hydrogen is projected not only as an industrial commodity but also as a clean energy vector for decarbonizing the transportation sector [21]. Hydrogen has unique combustion characteristics, including high laminar flame velocity and substantial energy content per unit mass. Its addition has been shown to increase thermal efficiency beyond that of single-fuel diesel engines [8]; however, its rapid combustion characteristics inevitably lead to sharp increases in in-cylinder temperature, thereby drastically intensifying nitrogen-based emissions, particularly $NO_x$ [16].

To mitigate $NO_x$ emissions in hydrogen-fueled engines, EGR is often used as a control strategy. EGR operates by recirculating a portion of exhaust gases back into the combustion chamber, thereby reducing oxygen concentration and peak combustion temperature [13]. Nevertheless, the primary challenge of EGR implementation lies in the potential penalties on combustion efficiency and operational stability if its ratio is not precisely optimized relative to the main fuel supply.

Recent studies have extensively explored hydrogen-enrichment strategies across various flow rates. Sathyamurthy et al. investigated low-to-medium flow ranges (0–10 LPM). They reported that hydrogen induction consistently improved thermal efficiency beyond levels achieved with biodiesel, albeit accompanied by sharp increases in $NO_x$ emissions [27, 32]. These findings were reinforced by Elnajjar et al., who extended the operating range up to 18.4 LPM, achieving substantial performance gains but with increasingly unavoidable $NO_x$ risks [3]. To counteract this escalation, EGR techniques have been applied in several dual-fuel studies. Kannappan et al. tested a constant hydrogen flow (6 LPM) combined with varying EGR levels (10% and 20%) in a Syzygium cumini biodiesel engine, recording

$NO_x$ reductions of up to 25% compared to non-EGR operation. However, performance declined slightly relative to diesel single fuel (B100 and D100) at full load [13]. Similarly, Zhang et al. optimized a broader EGR range (0–30%), concluding that while EGR effectively suppressed $NO_x$, levels above 20% tended to worsen soot emissions [34]. Meanwhile, Marikatti et al. highlighted that EGR addition (10–20%) successfully mitigated hydrogen explosive combustion behavior, though stability at low loads remained challenging compared to the steadiness of mono-fuel diesel flames [19].

Recent research has begun using advanced statistical methods and fundamental analysis of low-carbon fuels to optimize the diesel dual-fuel engines. Bora et al. demonstrated that analysis of variance (ANOVA) effectively maps the nonlinear relationship between engine load and injection pressure, achieving optimal thermal efficiency (BTE) in a hydrogen-powered engine [11]. Meanwhile, a comparative study by Grab-Rogaliński et al. found that hydrogen enrichment improves thermal efficiency but doubles $NO_x$ emissions via thermal mechanisms, driven by higher combustion temperatures [8]. These studies lay a solid foundation for optimizing injection parameters and understanding emission mechanisms. However, a gap remains in describing how hydrogen flow and EGR mitigation strategies interact simultaneously.

To address this gap, this study offers a more comprehensive approach. Its originality lies in testing specific combinations of hydrogen flow and EGR levels while quantitatively describing their interaction in one integrated experiment. The study aims to use statistical analysis (ANOVA and Tukey's HSD) to map the synergistic effect between hydrogen enrichment and EGR application and to identify precise 'compensation points'. The focus is on quantifying the trade-off between energy efficiency and pollutant reduction, so hydrogen-induced $NO_x$ emissions can be reduced without compromising engine thermal performance at specific operating conditions.

## 2. Material and method

This section details the experimental apparatus and methodological framework used to evaluate the combined effects of hydrogen induction and EGR on a CI engine fueled with biodiesel. The investigation was designed to systematically quantify the trade-offs between performance parameters (BP, BSFC, BTE) and $NO_x$ emissions. The specifications of the test fuels, standard engine configuration, instrumentation accuracy, and the statistical design of the experiment are described in the following subsections.

### 2.1. Fuel properties and preparation

This experimental investigation is focused on the exclusive use of renewable fuels. The primary liquid fuel employed is pure Palm Oil Methyl Ester (POME) or B100 biodiesel, while hydrogen gas ($H_2$) is introduced as an energy supplement through the intake system. The B100 biodiesel used in this study was produced from crude palm oil (CPO) as the raw material.

In this work, engine operation with pure B100 (without hydrogen) is established as the baseline condition to evaluate the effectiveness of hydrogen supplementation and EGR intervention. The physicochemical properties of B100 and hydrogen utilized in the tests are summarized in Table 1.

Table 1. Fuel properties

| Properties | Unit | POME CPO (B100) | Hydrogen ($H_2$) |
|---|---|---|---|
| Density 15°C | kg/m³ | 870 | 0.089 |
| Kinematic viscosity 40°C | mm²/s (cSt) | 4.5 | 0 |
| Lower heating value | MJ/kg | 39.910 | 119.810 |
| Cetane number | – | 55 | – |
| Flash point | °C | 170 | – |
| Auto ignition temperature | °C | > 101 | 585 |
| Stoichiometric air-fuel ratio | – | 12,5 | 34.3 |

### 2.2. Experimental setup

The central experimental unit consists of a single-cylinder, four-stroke, water-cooled Diamond DI 800 H diesel dual fuel engine with direct injection. The engine is coupled with an Eddy Current Dynamometer to vary the engine load during testing. In line with the study focus on practical applicability, the engine was maintained in its original factory configuration. No mechanical modifications were made to the compression ratio, fuel injection timing, or combustion chamber geometry. The engine technical specifications are presented in Table 2.

Table 2. Diamond DI 800 H engine specifications

| Parameter | Specifications |
|---|---|
| Brand & model | Diamond DI 800 H |
| Engine type | 1-cylinder, 4-stroke, horizontal, water cooled |
| Combustion system | Direct injection |
| Bore x stroke | 82 mm x 78 mm |
| Cylinder volume (displacement) | 411 cc |
| Compression ratio | 18 : 1 |
| Maximum power (max output) | 5.96 kW at 2400 rpm |
| Rated power (rated output) | 5.22 kW at 2200 rpm |
| Max torque | 25.5 Nm at 1900 rpm |
| Cooling system | Hopper type |
| Lubrication system | Trochoid type |
| Pilot injection timing | 13 BTDC |
| Rotation direction | Counter-clockwise |

Modifications were made to the air intake system to accommodate dual-fuel operation and EGR. A schematic of the experimental setup is shown in Fig. 1.

Hydrogen gas is supplied from a high-pressure cylinder (200 bar) equipped with a two-stage pressure regulator. To ensure precise flow control, hydrogen is directed through a Digital Mass Flow Controller (MFC) with a measurement range of 0–20 LPM (accuracy: ±1% FS). The hydrogen is then injected into the intake manifold using the fumigation technique (continuous port injection). For safety purposes, a flashback arrestor is installed along the hydrogen supply line to prevent flashback from the combustion chamber.

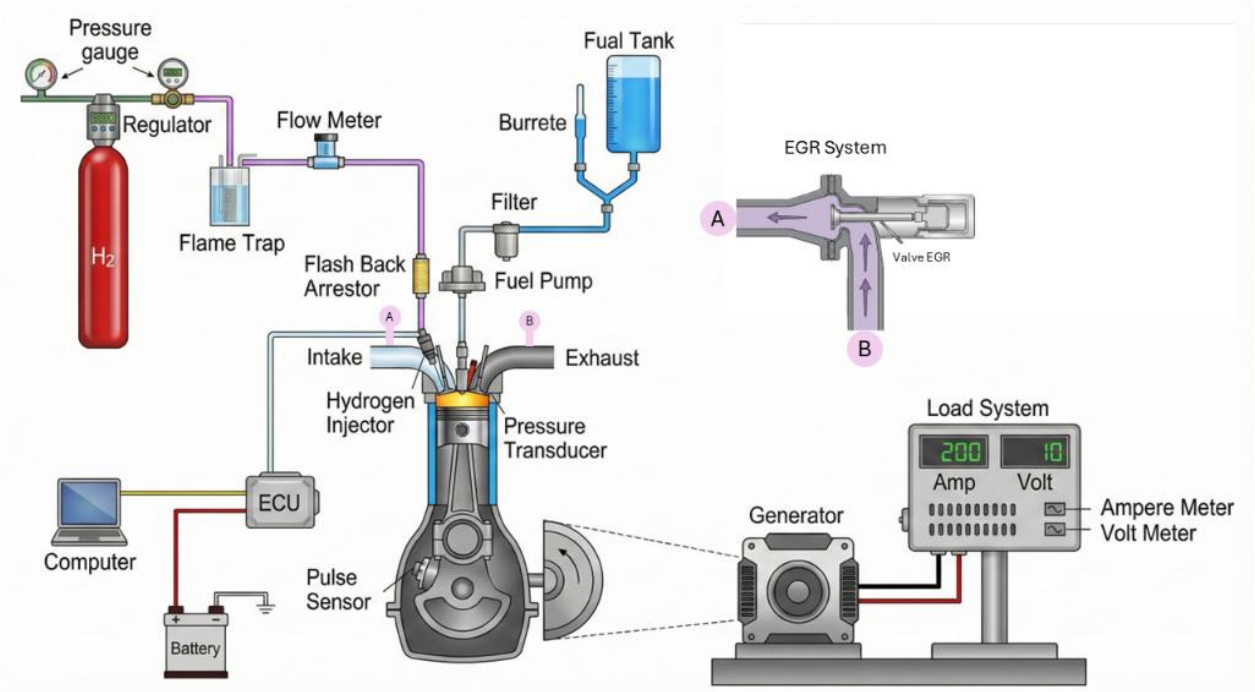


Fig. 1. Experimental setup

Table 3. Test instrument specifications

| Generator electrical dynamometer | | Gas mass flowmeter | | Gas analyzer | | Burette | |
|---|---|---|---|---|---|---|---|
| Type | ST-6 | Type | MF5712 (air flow meter) | Type | Gas analyzer (EPSG5) | Type | Pyrex |
| Volt-age/current | 230 V / 26.1 A (AC) | Flow range | 0–200 SLPM | Gas measurement | CO, HC, $CO_2$, $O_2$, $NO_x$, Lamda | Measure range | 0–100 mL |
| Max. AC output | 6 kW | Accuracy | ±(2.0% + 0.5% FS) | $NO_x$ measurement range | 0–5000 ppm | Accuracy | 0.05 mL |
| Frequency | 50 Hz | Repeatability | ±0.5% FS | Accuracy | 1 ppm | | |
| Loading system | Electric bulb system | Turn-down ratio | 30:1 | Response time | 10 s | | |
| Electric control | Volt meter, amperemeter, switch | Response time | ≤ 2 s | Power consumption | 50 W at 110–220 V | | |

The EGR system employed is of the external low-pressure loop type. A bypass pipeline connects the exhaust manifold back to the intake manifold, positioned immediately after the air filter but before the hydrogen injection point. The EGR flow rate is manually regulated using a precision gate valve.

### 2.3. Instrumentation and data acquisition

The technical specifications of the leading equipment used for engine loading, fuel flow rate measurement, and exhaust gas emission analysis are summarized in Table 3.

### 2.4. Design of experiment & test procedure

The experimental design (DoE) in this study is focused on investigating the influence of two main independent variables, namely hydrogen flow rate and EGR level, on the characteristics of a diesel dual fuel engine. All tests were conducted under a constant load of 2 kW to ensure consistent comparison of thermal performance and emissions. Hydrogen flow rates were varied at 2.5, 5.0, and 7.5 LPM, while EGR levels were set at 5%, 10%, and 15%. Operational data from biodiesel mode (single-fuel) without EGR were first recorded as baseline data to evaluate the effectiveness of energy substitution and emission-reduction strategies.

The testing procedure began with a thorough inspection of measurement instruments and calibration of the gas analyzer under ambient air conditions (zeroing). The engine was then warmed up for 15–20 minutes, until the coolant temperature reached a stable operating range (70–80°C). Once thermal stability was achieved, a 2 kW electrical load was gradually applied through the dynamometer generator. During data acquisition, hydrogen gas was injected into the intake manifold at specified flow rates (2.5, 5.0, and 7.5 LPM) using a Mass Flow Meter. After the engine speed stabilized, the EGR valve was manually opened to achieve the target EGR levels (5%, 10%, and 15%). Fuel consumption, electrical parameters, and exhaust emissions were recorded only when the engine had reached steady-state conditions for at least 3 minutes at each test point combination.

The procedure concluded by shutting off the hydrogen supply, closing the EGR valve, releasing the engine load, and allowing the engine to run at idle for cooling before being switched off.

### 2.5. Data processing and statistical analysis

The experimental data obtained from engine testing (engine performance: BP, BSFC, BTE and emissions: $NO_x$) were analyzed using statistical methods to evaluate the influence of the independent variables (hydrogen flow and EGR rate) on the dependent variables. All statistical analyses were conducted at a 95% confidence level (alpha = 0.05) using Minitab statistical software. The data analysis procedure was carried out in three main stages: (1) verification of assumption checks, (2) analysis of variance (ANOVA), and (3) Post-hoc analysis [22].

The following hypotheses were formulated for this analysis:

– Normality
  $H_0$ : The residuals are normally distributed
  $H_1$ : The residuals are not normally distributed
– Constant variance
  $H_0$ : $\sigma_{11}^2 = \sigma_{12}^2 = \sigma_{13}^2 = \sigma_{21}^2 = \sigma_{22}^2 = \sigma_{23}^2$
  $H_1$ : At least one $\sigma^2$ is different
– ANOVA
  Hydrogen Flow
  $H_0$ : $\tau_1, \tau_2, \tau_3 = 0$
  $H_1$ : At least one $\tau_1, \tau_2, \tau_3 \neq 0$
  EGR
  $H_0$ : $\beta_1, \beta_2, \beta_3 = 0$
  $H_1$ : At least one $\beta_1, \beta_2, \beta_3 \neq 0$
  Interaction (Hydrogen Flow*EGR)
  $H_0$ : $\tau\beta_{ij} = 0$
  $H_1$ : $\tau\beta_{ij} \neq 0$
– Post-hoc (comparison)
  Hydrogen Flow
  $H_0$ : $\mu_{i1} = \mu_{i2}$
  $H_1$ : $\mu_{i1} \neq \mu_{i2}$
  EGR
  $H_0$ : $\mu_{j1} = \mu_{j2}$
  $H_1$ : $\mu_{j1} \neq \mu_{j2}$
  Interaction (Hydrogen Flow*EGR)
  $H_0$ : $\mu_{ij} = \mu_{ij}$
  $H_1$ : $\mu_{ij} \neq \mu_{ij}$

## 3. Result and discussion

The quantitative data obtained from the acquisition system were averaged to ensure reliability. The recapitulation of the experimental results for all test configurations is presented in Table 4. This dataset serves as the quantitative foundation for the subsequent statistical analysis.

### 3.1. Statistical check assumptions

#### 3.1.1. Normality test

The validity of the statistical model was first evaluated by testing the normality of residuals to ensure the appropriateness of applying parametric ANOVA methods. This assessment was conducted using the Normal Probability Plot technique and the Anderson-Darling statistical test [22]. Based on the analysis results in Table 5, the mean residual values for all response parameters were minimal, approaching zero (ranging from $10^{-14}$ to $10^{-16}$). Furthermore, the P-values obtained for each variable were 0.593 for BP, 0.588 for BTE, 0.824 for BSFC, and 0.198 for $NO_x$ emissions. Since all P-values were significantly greater than the predetermined significance level (alpha = 0.05), the null hypothesis ($H_0$) was accepted. Accordingly, it was concluded that the residual data are typically distributed, thereby fulfilling the fundamental assumption required for variance analysis (ANOVA).

Table 4. Experimental design matrix and average response values

| Run order | Hydrogen Flow [l/m] | EGR [%] | BP [kW] | BSFC [g/kWh] | BTE [%] | $NO_x$ [ppm] |
|---|---|---|---|---|---|---|
| 1 | 2.5 | 15 | 2.095 | 339.73 | 21.43 | 175.629 |
| 2 | 5 | 10 | 2.184 | 262.87 | 21.54 | 280.783 |
| 3 | 5 | 5 | 2.2 | 276.92 | 20.9 | 298.768 |
| 4 | 7.5 | 10 | 2.191 | 238.11 | 19.14 | 315.345 |
| 5 | 2.5 | 5 | 2.18 | 366 | 20.31 | 280.929 |
| 6 | 5 | 5 | 2.203 | 276.03 | 20.95 | 295.877 |
| 7 | 5 | 15 | 2.178 | 258.51 | 21.74 | 285.928 |
| 8 | 5 | 15 | 2.173 | 259.45 | 21.68 | 286.928 |
| 9 | 5 | 10 | 2.184 | 264.53 | 21.45 | 279.783 |
| 10 | 7.5 | 15 | 2.163 | 238.49 | 19 | 287.232 |
| 11 | 2.5 | 5 | 2.183 | 371.19 | 20.08 | 278.726 |
| 12 | 2.5 | 10 | 2.126 | 328.25 | 22.09 | 227.687 |
| 13 | 2.5 | 10 | 2.132 | 343.3 | 21.32 | 228.935 |
| 14 | 2.5 | 5 | 2.175 | 352.63 | 20.93 | 284.937 |
| 15 | 5 | 15 | 2.168 | 262.13 | 21.52 | 284.928 |
| 16 | 7.5 | 10 | 2.197 | 236.44 | 19.24 | 310.614 |
| 17 | 2.5 | 10 | 2.125 | 335.98 | 21.68 | 231.952 |
| 18 | 7.5 | 15 | 2.165 | 237.57 | 19.05 | 285.939 |
| 19 | 7.5 | 10 | 2.184 | 239.08 | 19.07 | 312.456 |
| 20 | 7.5 | 5 | 2.213 | 245.92 | 18.92 | 348.238 |
| 21 | 7.5 | 15 | 2.176 | 235.2 | 19.19 | 270.925 |
| 22 | 7.5 | 5 | 2.216 | 243.14 | 19.05 | 347.439 |
| 23 | 2.5 | 15 | 2.071 | 337.74 | 21.48 | 168.763 |
| 24 | 5 | 5 | 2.207 | 277.44 | 20.89 | 292.345 |
| 25 | 5 | 10 | 2.182 | 265.42 | 21.4 | 281.783 |
| 26 | 7.5 | 5 | 2.22 | 239.99 | 19.19 | 345.938 |
| 27 | 2.5 | 15 | 2.089 | 337.19 | 21.54 | 177.136 |

Table 5. Normality test

| Response | Mean | P-value |
|---|---|---|
| BP | $-1.315852 \times 10^{-16}$ | 0.593 |
| BSFC | $-1.779365 \times 10^{-16}$ | 0.588 |
| BTE | $6.227376 \times 10^{-14}$ | 0.824 |
| $NO_x$ | $-9.789701 \times 10^{-14}$ | 0.198 |

### 3.1.2. Constant variance

Subsequently, the homogeneity of variance across treatment groups (Hydrogen Flow Rate and EGR) was verified using Levene's test [22]. Based on the statistical results in Table 6, the P-values obtained for each response were 0.695 (BP), 0.200 (BSFC), 0.234 (BTE), and 0.737 ($NO_x$ emissions). All probability values were well above the alpha = 0.05 significance threshold, indicating that the variances among treatment groups were uniform and not significantly different. Therefore, the null hypothesis (H0) was accepted, and the assumption of variance homogeneity was confirmed for all tested parameters, thereby validating the application of ANOVA for further comparative analysis.

Table 6. Constant variance test

| Response | Test Statistic | P-value |
|---|---|---|
| BP | 0.69 | 0.695 |
| BSFC | 1.58 | 0.200 |
| BTE | 1.48 | 0.234 |
| $NO_x$ | 0.64 | 0.737 |

### 3.1.3. Independent test

The independence of residuals was verified using Residuals versus Observation Order plots to detect potential autocorrelation or time-related bias during the experiment. This assumption requires that errors between observations are uncorrelated, as indicated by random fluctuations without cyclic patterns or temporal trends [22]. Based on visual evaluation of the BP, BTE, BSFC, and $NO_x$ plots, the residuals were observed to scatter stochastically around the zero line throughout the testing sequence. No systematic patterns, consistent upward or downward trends, or indications of long runs suggesting data dependence were detected. The absence of serial correlation confirms that each data acquisition was independent, thereby fully satisfying the ANOVA model independence assumption [4].

### 3.1.4. Residual versus fitted values

Finally, the Residuals versus Fitted Values plots were analyzed to detect signs of heteroscedasticity and to verify the independence of error variance. Theoretically, a valid model is characterized by residuals that are randomly scattered around the zero line, without forming any specific geometric patterns [22]. Based on visual inspection of the four response parameters (BP, BTE, BSFC, and $NO_x$), all plots exhibited randomly distributed residuals with no structural patterns. No funnel-shaped or megaphone-like widening trends were observed with increasing fitted values, which are typical of unequal variance. The absence of systematic patterns confirms that the constant variance assumption is fully satisfied, thereby reinforcing the robustness of the ANOVA model for further interpretation [1].

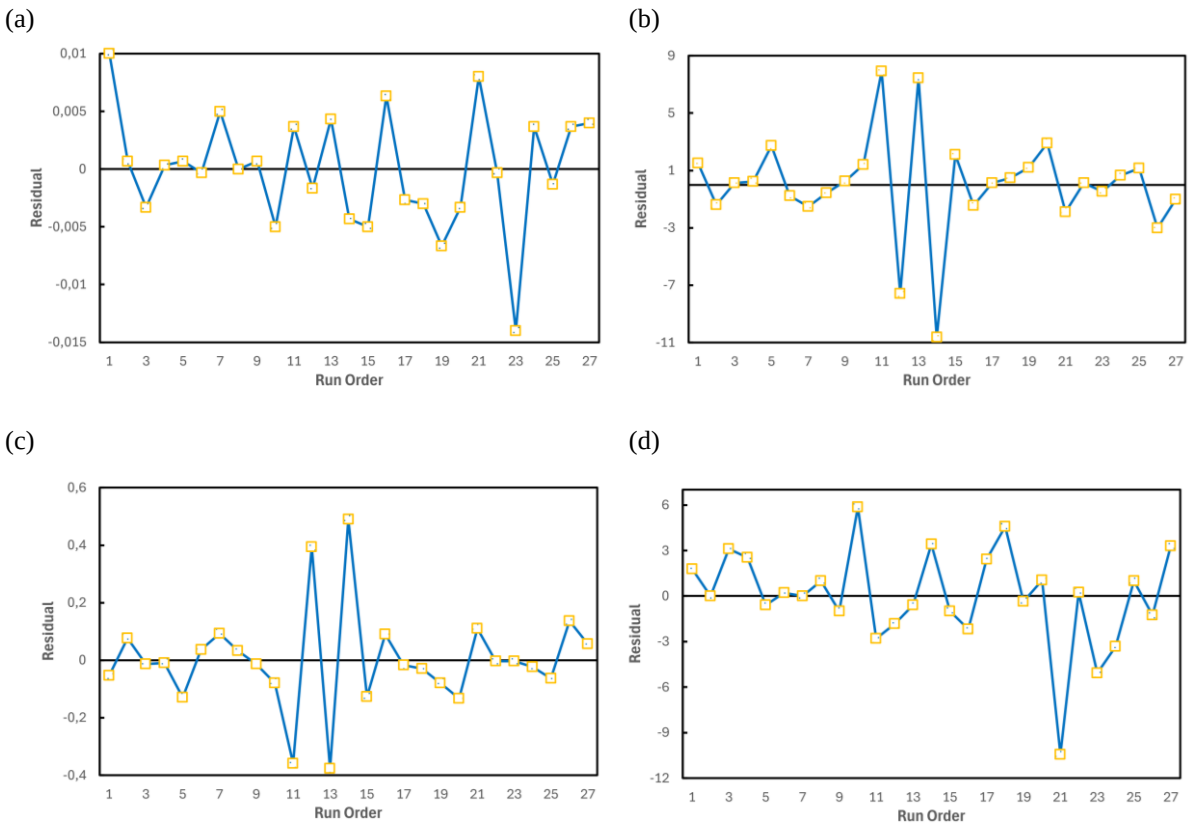


Fig. 2. Independent test result graphs: (a) BP, (b) BSFC, (c) BTE, (d) $NO_x$

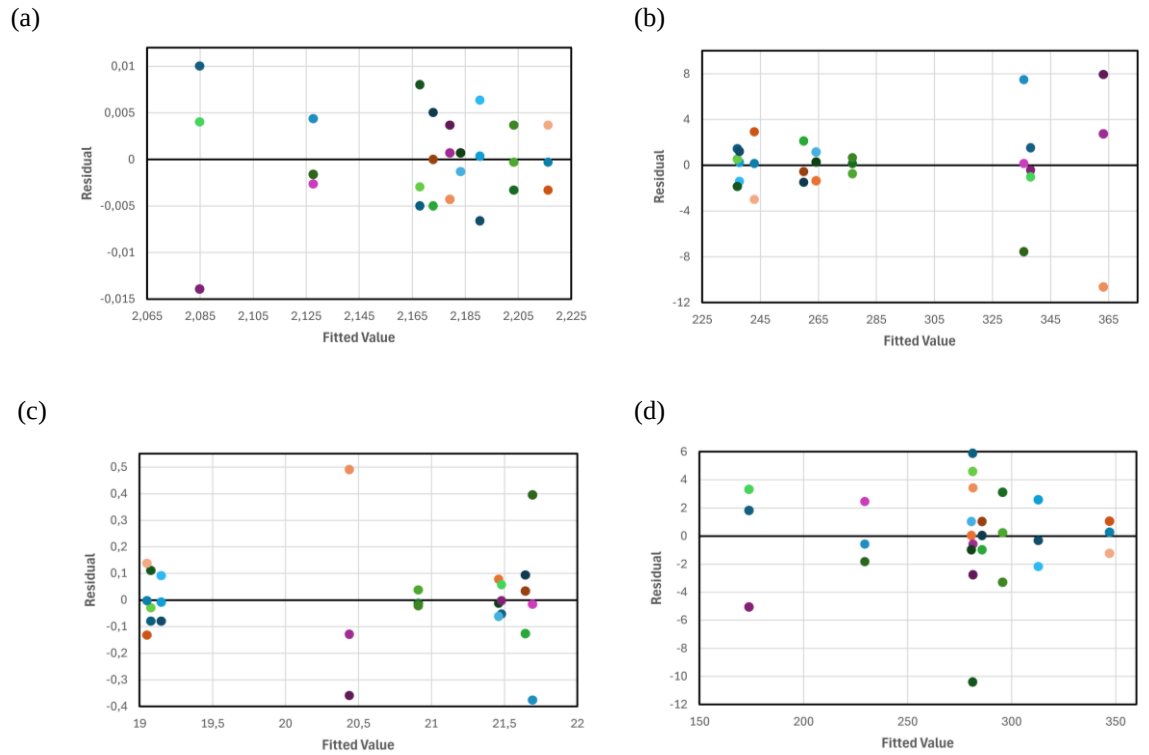


Fig. 3. Plot of residual results versus fitted value: (a) BP, (b) BSFC, (c) BTE, (d) $NO_x$

Table 7. Summary of ANOVA results for performance and emission parameters

| Analysis of variance | | | | | | | | |
|---|---|---|---|---|---|---|---|---|
| Factor (X) | BP | | BSFC | | BTE | | $NO_x$ | |
| Source | F-Value | P-Value | F-Value | P-Value | F-Value | P-Value | F-Value | P-Value |
| Hydrogen flow | 281.93 | 0.000 | 1459.3 | 0.000 | 322.34 | 0.000 | 1139.99 | 0.000 |
| EGR | 205.75 | 0.000 | 38.28 | 0.000 | 25.88 | 0.000 | 556.83 | 0.000 |
| Hydrogen flow*EGR | 22.44 | 0.000 | 6.16 | 0.003 | 7.37 | 0.001 | 122.18 | 0.000 |

### 3.2. Engine performance and emission ANOVA analysis

The analysis of variance (ANOVA) results in Table 7 statistically confirm that hydrogen injection, EGR rate, and their interaction significantly influence all response parameters ($P < 0.05$).

Specifically, hydrogen flow was identified as the most dominant factor affecting BSFC, as indicated by the extreme F-value of 1459.3. This dominance suggests that substituting liquid fuel with hydrogen significantly improves fuel consumption efficiency. a phenomenon consistent with hydrogen's higher specific heat of combustion than biodiesel [29].

Meanwhile. for $NO_x$ emissions. both primary variables demonstrated nearly equivalent levels of influence. although Hydrogen Flow ($F = 1139.99$) remained slightly more dominant than EGR ($F = 556.83$). The magnitude of these F-values confirms the presence of a competing mechanism within the combustion chamber: hydrogen tends to elevate combustion temperature. thereby promoting thermal $NO_x$ formation [28]. At the same time. EGR effectively suppresses this temperature rise through its thermal dilution effect [34].

The most noteworthy finding lies in the significance of the interaction effect (Hydrogen Flow*EGR). With P-values of 0.003 across all responses. The results demonstrate that the influence of hydrogen supplementation on engine performance and emissions does not operate independently. But it is highly dependent on the level of EGR applied (and vice versa), for instance, in the case of $NO_x$ emissions. The high interaction F-value (122.18) indicates that the effectiveness of EGR in reducing emissions varies nonlinearly with the amount of hydrogen injected. This validates the importance of simultaneous optimization strategies in this study to identify the optimal trade-off point between high performance and low emissions, as highlighted in previous literature [14].

### 3.3. Post ANOVA (comparison)

#### 3.3.1. Brake power

Multiple-comparison testing using Tukey's Simultaneous Tests was conducted to identify specific mean differences and determine the optimal operating configuration for Brake Power (BP), as summarized in Table 8. Increasing hydrogen flow from 2.5 LPM to 5.0 LPM significantly improved performance ($T = 19.61$, $P < 0.05$). confirming that initial hydrogen injection effectively boosts combustion pressure. However further increasing the flow to 7.5 LPM did not yield a significant difference ($P = 0.200$). This suggests a saturation point where excessive hydrogen displaces intake air. reducing volumetric efficiency and offset-

ting hydrogen's calorific advantage due to limited oxygen availability [9]. Consequently. 5.0 LPM is identified as a more efficient operating point than 7.5 LPM.

Regarding EGR levels. negative T-values consistently indicated significant reductions in BP compared to baseline ($P < 0.05$). The most substantial reduction occurred at 10% EGR ($T = –20.23$). where the dilution effect of exhaust gases suppressed the fuel oxidation rate and the peak cycle temperature. thereby reducing piston work [17].

Interaction analysis revealed critical trade-off phenomena. Notably. the performance of (5.0 $H_2$. 10% EGR) and (2.5 $H_2$. 5% EGR) was statistically identical ($P = 0.995$). demonstrating that increasing hydrogen to 5.0 LPM can compensate for the power loss caused by doubling the EGR rate. Hydrogen successfully restores the combustion reactivity suppressed by inert gases [20]. Conversely. at 15% EGR. Increasing hydrogen from 5.0 to 7.5 LPM was ineffective ($P = 0.979$). reinforcing that excessive hydrogen cannot overcome high dilution levels. Thus. 5.0 LPM of hydrogen is recommended as the optimum limit, as higher flow rates do not provide statistically significant gains. especially when combined with EGR.

Table 8. Post ANOVA (comparison) BP response

| Tukey Simultaneous Tests for Differences of Means | Source | T-value | P-value |
|---|---|---|---|
| Difference of Hydrogen Flow Level | 5.0–2.5 | 19.61 | 0.000 |
| | 7.5–2.5 | 21.4 | 0.000 |
| | 7.5–5.0 | 1.79 | 0.200 |
| Difference of Hydrogen Flow Level | 5 | –11.38 | 0.000 |
| | 10 | –20.23 | 0.000 |
| | 15 | –8.85 | 0.000 |
| Difference of Hydrogen Flow*EGR Level | (2.5 10)–(2.5 5) | –10.47 | 0.000 |
| | (2.5 15)–(2.5 5) | –19.11 | 0.000 |
| | (5.0 5)–(2.5 5) | 4.86 | 0.003 |
| | (5.0 10)–(2.5 5) | 0.81 | 0.995 |
| | (5.0 15)–(2.5 5) | –1.28 | 0.924 |
| | (7.5 5)–(2.5 5) | 7.49 | 0.000 |
| | (7.5 10)–(2.5 5) | 2.3 | 0.393 |
| | (7.5 15)–(2.5 5) | –2.3 | 0.393 |
| | (2.5 15)–(2.5 10) | –8.64 | 0.000 |
| | (5.0 5)–(2.5 10) | 15.33 | 0.000 |
| | (5.0 10)–(2.5 10) | 11.28 | 0.000 |
| | (5.0 15)–(2.5 10) | 9.18 | 0.000 |
| | (7.5 5)–(2.5 10) | 17.96 | 0.000 |
| | (7.5 10)–(2.5 10) | 12.76 | 0.000 |
| | (7.5 15)–(2.5 10) | 8.17 | 0.000 |
| | (5.0 5)–(2.5 15) | 23.97 | 0.000 |
| | (5.0 10)–(2.5 15) | 19.92 | 0.000 |
| | (5.0 15)–(2.5 15) | 17.83 | 0.000 |
| | (7.5 5)–(2.5 15) | 26.6 | 0.000 |
| | (7.5 10)–(2.5 15) | 21.4 | 0.000 |
| | (7.5 15)–(2.5 15) | 16.81 | 0.000 |
| | (5.0 10)–(5.0 5) | –4.05 | 0.017 |
| | (5.0 15)–(5.0 5) | –6.14 | 0.000 |
| | (7.5 5)–(5.0 5) | 2.63 | 0.239 |
| | (7.5 10)–(5.0 5) | –2.57 | 0.266 |
| | (7.5 15)–(5.0 5) | –7.16 | 0.000 |
| | (5.0 15)–(5.0 10) | –2.09 | 0.506 |
| | (7.5 5)–(5.0 10) | 6.68 | 0.000 |
| | (7.5 10)–(5.0 10) | 1.49 | 0.848 |
| | (7.5 15)–(5.0 10) | –3.11 | 0.106 |
| | (7.5 5)–(5.0 15) | 8.78 | 0.000 |
| | (7.5 10)–(5.0 15) | 3.58 | 0.043 |
| | (7.5 15)–(5.0 15) | –1.01 | 0.979 |
| | (7.5 10)–(7.5 5) | –5.2 | 0.002 |
| | (7.5 15)–(7.5 5) | –9.79 | 0.000 |
| | (7.5 15)–(7.5 10) | –4.59 | 0.005 |

Table 9. Post ANOVA (comparison) BSFC response

| Tukey Simultaneous Tests for Differences of Means | Source | T-value | P-value |
|---|---|---|---|
| Difference of Hydrogen Flow Level | 5.0–2.5 | –38.51 | 0.000 |
| | 7.5–2.5 | –52.07 | 0.000 |
| | 7.5–5.0 | –13.55 | 0.000 |
| Difference of Hydrogen Flow Level | 5 | –7.35 | 0.000 |
| | 10 | –7.78 | 0.000 |
| | 15 | –0.43 | 0.902 |
| Difference of Hydrogen Flow*EGR Level | (2.5 10)–(2.5 5) | –7.75 | 0.000 |
| | (2.5 15)–(2.5 5) | –7.07 | 0.000 |
| | (5.0 5)–(2.5 5) | –24.42 | 0.000 |
| | (5.0 10)–(2.5 5) | –27.96 | 0.000 |
| | (5.0 15)–(2.5 5) | –29.15 | 0.000 |
| | (7.5 5)–(2.5 5) | –33.96 | 0.000 |
| | (7.5 10)–(2.5 5) | –35.41 | 0.000 |
| | (7.5 15)–(2.5 5) | –35.63 | 0.000 |
| | (2.5 15)–(2.5 10) | 0.67 | 0.999 |
| | (5.0 5)–(2.5 10) | –16.67 | 0.000 |
| | (5.0 10)–(2.5 10) | –20.21 | 0.000 |
| | (5.0 15)–(2.5 10) | –21.41 | 0.000 |
| | (7.5 5)–(2.5 10) | –26.21 | 0.000 |
| | (7.5 10)–(2.5 10) | –27.66 | 0.000 |
| | (7.5 15)–(2.5 10) | –27.89 | 0.000 |
| | (5.0 5)–(2.5 15) | –17.34 | 0.000 |
| | (5.0 10)–(2.5 15) | –20.88 | 0.000 |
| | (5.0 15)–(2.5 15) | –22.08 | 0.000 |
| | (7.5 5)–(2.5 15) | –26.88 | 0.000 |
| | (7.5 10)–(2.5 15) | –28.34 | 0.000 |
| | (7.5 15)–(2.5 15) | –28.56 | 0.000 |
| | (5.0 10)–(5.0 5) | –3.54 | 0.047 |
| | (5.0 15)–(5.0 5) | –4.73 | 0.004 |
| | (7.5 5)–(5.0 5) | –9.54 | 0.000 |
| | (7.5 10)–(5.0 5) | –10.99 | 0.000 |
| | (7.5 15)–(5.0 5) | –11.21 | 0.000 |
| | (5.0 15)–(5.0 10) | –1.2 | 0.947 |
| | (7.5 5)–(5.0 10) | –6 | 0.000 |
| | (7.5 10)–(5.0 10) | –7.45 | 0.000 |
| | (7.5 15)–(5.0 10) | –7.68 | 0.000 |
| | (7.5 5)–(5.0 15) | –4.8 | 0.004 |
| | (7.5 10)–(5.0 15) | –6.26 | 0.000 |
| | (7.5 15)–(5.0 15) | –6.48 | 0.000 |
| | (7.5 10)–(7.5 5) | –1.45 | 0.863 |
| | (7.5 15)–(7.5 5) | –1.67 | 0.754 |
| | (7.5 15)–(7.5 10) | –0.22 | 1.000 |

**3.3.2 Brake specific fuel consumption**

In contrast to the saturation observed in BP. the multiple-comparison analysis for BSFC shows a linear. monotonic improvement trend (Table 9). For instance. transitions from 2.5 LPM to 5.0 LPM. and further to 7.5 LPM. consistently yielded significant reductions in fuel consumption ($P < 0.001$. $T = –38.51$ and $–13.55$). This sustained improvement is primarily driven by hydrogen's high Lower Heating Value (~120 MJ/kg); substituting liquid fuel with a lighter. More energetic gaseous fuels naturally lower the mass-to-energy ratio (g/kWh) [18]. Furthermore. hydrogen's high diffusivity promotes more complete combustion. ensuring better energy conversion across all tested levels [15].

A notable finding in the interaction analysis is the diminishing influence of EGR at higher hydrogen substitution rates. Specifically. at 7.5 LPM of hydrogen. variations in EGR levels (5%. 10%. and 15%) no longer significantly impacted fuel consumption. evidenced by high P-values ($P = 1.000$ for the 15% vs. 10% comparison). These results suggest that at sufficient concentrations. Hydrogen's reactivity dominates the combustion characteristics. In this state the typical efficiency penalties associated with EGR. such as slower combustion or pumping losses. are effectively masked or mitigated by hydrogen's high thermal efficiency [17].

While the BP analysis suggested an optimal limit of 5.0 LPM due to volumetric efficiency trade-offs, the BSFC results indicate that 7.5 LPM remains the superior choice for fuel economy. However, the engines sensitivity to EGR becomes more apparent at lower hydrogen flows. For example. at 2.5 LPM. Increasing EGR from 5% to 10% significantly altered BSFC ($P < 0.001$). Though further increases to 15% showed no significant change ($P = 0.999$). This indicates that. while a minimal hydrogen supply initially makes the engine susceptible to EGR-induced disturbances. It eventually reaches a tolerance threshold [26]. Overall, high hydrogen concentrations provide a "shielding" effect. allowing for more flexible emission control strategies without compromising fuel economy.

**3.3.3 Brake thermal efficiency**

Post-hoc analysis in Table 10 reveals a distinct thermal behavior: an increase in the hydrogen energy fraction does not always translate into improved thermal efficiency, unlike the linear improvement observed in BSFC. BTE exhibits a clear operational limit. Tukey test results indicate that BTE reaches its optimum within the low-to-medium injection range. The comparison between 2.5 LPM and 5.0 LPM hydrogen flow yielded a T-value of 1.35 with a P-value of 0.385. This lack of statistical significance suggests that increasing the hydrogen supply within this range does not provide a meaningful boost to energy conversion efficiency.

A more critical shift occurs at 7.5 LPM, where a sharp decline in performance is observed. This is confirmed by large negative T-values ($–21.28$ and $–22.63$) and $P < 0.001$ when compared to both the 2.5 and 5.0 LPM levels. This phenomenon indicates that at 7.5 LPM, the engine experiences reduced volumetric efficiency due to the high volume of hydrogen displacing intake air. The air-fuel ratio deviates from the optimal combustion point. resulting in reduced energy conversion despite hydrogen's high calorific value [9].

One of the most compelling findings from this analysis is the interaction behavior under high-hydrogen conditions. At a flow rate of 7.5 LPM. variations in EGR levels (5% to 15%) had no impact on BTE, as evidenced by "perfect" P-values of 1.000 across these comparisons. This suggests that at high concentrations. hydrogen combustion becomes so dominant that it effectively overrides the thermodynamic effects typically associated with EGR.

In contrast, at a lower flow of 2.5 LPM, the engine remains highly sensitive to EGR changes ($P < 0.001$ for the 5% vs. 10% EGR comparison). This implies that when the hydrogen proportion is small. diesel diffusion mechanisms still govern the combustion process, which are inherently susceptible to the presence of inert gases.

In summary. to maximize thermal efficiency while maintaining reasonable fuel consumption. An operating range of 2.5–5.0 LPM is recommended. Using 7.5 LPM of hydrogen should be avoided, as it results in a significant loss in conversion efficiency.

**3.3.4 Nitrogen oxide**

Post-hoc analysis of $NO_x$ emissions reveals a critical thermal interaction between hydrogen enrichment and EGR. While previous sections focused on performance. This analysis evaluates the strategic mitigation of environmental impacts. Notably, the Tukey test results in Table 10 confirm a strong positive correlation between hydrogen flow and $NO_x$ formation. Comparisons across all hydrogen levels (2.5, 5.0, and 7.5 LPM) yielded significant increases ($P < 0.001$), with T-values reaching 46.62. This trend is a direct consequence of hydrogen's high adiabatic flame temperature. which accelerates the heat release rate and creates localized temperature spikes. These conditions promote thermal NOx formation via the Zeldovich mechanism in an exponential manner [23]. Without EGR intervention, the high hydrogen flow rate (7.5 LPM) would likely result in emissions exceeding regulatory standards.

Importantly, a fundamental finding of this study is EGR's capacity to neutralize the $NO_x$ increases induced by hydrogen. Specifically, interaction analysis demonstrates a precise compensation pattern; for instance. While $NO_x$ rose significantly at 5.0 LPM of hydrogen under low EGR, increasing the EGR rate to 10% restored emissions to baseline levels. This is evidenced by the comparison between (5.0 $H_2$ 10% EGR) and the baseline (2.5 $H_2$ 5% EGR), which yielded a P-value of 1.000. This statistical equality indicates that the heat-absorbing capacity of 10% EGR effectively offsets the thermal effect of 5.0 LPM hydrogen. Similarly. at maximum hydrogen levels. applying 15% EGR to the 7.5 LPM hydrogen configuration resulted in an emission profile statistically identical to the baseline ($P = 1.000$, $T = –0.05$).

In contrast to the BTE analysis, where EGR lost its influence at high hydrogen concentrations, EGR remains highly effective for NOx reduction even at 7.5 LPM hydrogen. Specifically. comparisons within the 7.5 LPM group (e.g.. 15% vs. 5% EGR) showed substantial reductions ($P < 0.001$, $T = –20.73$). This confirms that the high specific heat capacity of exhaust gas constituents, particularly $CO_2$ and $H_2O$, remains capable of absorbing the intense heat of hydrogen combustion. These results align with Vellaiyan

[31]. confirming that EGR technology in biodiesel-hydrogen engines can significantly suppress nitrogen oxide formation. In summary, these results validate an adaptive control strategy: increasing hydrogen flow enhances performance (BP/BSFC). The EGR level must be raised proportionally to maintain NOx neutrality. Thus, the operating pairs of (5.0 LPM $H_2$ + 10% EGR) and (7.5 LPM $H_2$ + 15% EGR) are identified as optimal configurations for achieving high performance without compromising emission standards.

## 4. Conclusion

This study successfully evaluated the synergistic and antagonistic effects of hydrogen induction and EGR in a biodiesel–based diesel dual-fuel engine using a comprehensive statistical approach. Based on the experimental data analysis and hypothesis testing, several key conclusions can be drawn:

– Hydrogen induction proved to be a highly effective strategy for enhancing energy efficiency. The addition of hydrogen consistently reduced BSFC linearly, due to

Table 10. Post ANOVA (comparison) BTE response

| Tukey Simultaneous Tests for Differences of Means | Source | T-value | P-value |
|---|---|---|---|
| Difference of Hydrogen Flow Level | 5.0–2.5 | 1.35 | 0.385 |
| | 7.5–2.5 | –21.28 | 0.000 |
| | 7.5–5.0 | –22.63 | 0.000 |
| Difference of Hydrogen Flow Level | 5 | 6.39 | 0.000 |
| | 10 | 6.06 | 0.000 |
| | 15 | –0.34 | 0.940 |
| Difference of Hydrogen Flow*EGR Level | (2.5 10)–(2.5 5) | 7.31 | 0.000 |
| | (2.5 15)–(2.5 5) | 6.07 | 0.000 |
| | (5.0 5)–(2.5 5) | 2.75 | 0.197 |
| | (5.0 10)–(2.5 5) | 5.95 | 0.000 |
| | (5.0 15)–(2.5 5) | 7.02 | 0.000 |
| | (7.5 5)–(2.5 5) | –8.07 | 0.000 |
| | (7.5 10)–(2.5 5) | –7.5 | 0.000 |
| | (7.5 15)–(2.5 5) | –7.91 | 0.000 |
| | (2.5 15)–(2.5 10) | –1.24 | 0.936 |
| | (5.0 5)–(2.5 10) | –4.56 | 0.006 |
| | (5.0 10)–(2.5 10) | –1.36 | 0.900 |
| | (5.0 15)–(2.5 10) | –0.29 | 1.000 |
| | (7.5 5)–(2.5 10) | –15.38 | 0.000 |
| | (7.5 10)–(2.5 10) | –14.81 | 0.000 |
| | (7.5 15)–(2.5 10) | –15.22 | 0.000 |
| | (5.0 5)–(2.5 15) | –3.32 | 0.072 |
| | (5.0 10)–(2.5 15) | –0.12 | 1.000 |
| | (5.0 15)–(2.5 15) | 0.95 | 0.986 |
| | (7.5 5)–(2.5 15) | –14.13 | 0.000 |
| | (7.5 10)–(2.5 15) | –13.57 | 0.000 |
| | (7.5 15)–(2.5 15) | –13.98 | 0.000 |
| | (5.0 10)–(5.0 5) | 3.2 | 0.090 |
| | (5.0 15)–(5.0 5) | 4.27 | 0.011 |
| | (7.5 5)–(5.0 5) | –10.82 | 0.000 |
| | (7.5 10)–(5.0 5) | –10.26 | 0.000 |
| | (7.5 15)–(5.0 5) | –10.66 | 0.000 |
| | (5.0 15)–(5.0 10) | 1.07 | 0.972 |
| | (7.5 5)–(5.0 10) | –14.02 | 0.000 |
| | (7.5 10)–(5.0 10) | –13.46 | 0.000 |
| | (7.5 15)–(5.0 10) | –13.86 | 0.000 |
| | (7.5 5)–(5.0 15) | –15.08 | 0.000 |
| | (7.5 10)–(5.0 15) | –14.52 | 0.000 |
| | (7.5 15)–(5.0 15) | –14.93 | 0.000 |
| | (7.5 10)–(7.5 5) | 0.56 | 1.000 |
| | (7.5 15)–(7.5 5) | 0.16 | 1.000 |
| | (7.5 15)–(7.5 10) | –0.41 | 1 |

Table 11. Post ANOVA (comparison) $NO_x$ response

| Tukey Simultaneous Tests for Differences of Means | Source | T-value | P-value |
|---|---|---|---|
| Difference of Hydrogen Flow Level | 5.0–2.5 | 32.26 | 0.000 |
| | 7.5–2.5 | 46.62 | 0.000 |
| | 7.5–5.0 | 14.36 | 0.000 |
| Difference of Hydrogen Flow Level | 5 | –18.41 | 0.000 |
| | 10 | –33.31 | 0.000 |
| | 15 | –14.9 | 0.000 |
| Difference of Hydrogen Flow*EGR Level | (2.5 10)–(2.5 5) | –16.37 | 0.000 |
| | (2.5 15)–(2.5 5) | –33.9 | 0.000 |
| | (5.0 5)–(2.5 5) | 4.45 | 0.007 |
| | (5.0 10)–(2.5 5) | –0.24 | 1.000 |
| | (5.0 15)–(2.5 5) | 1.38 | 0.890 |
| | (7.5 5)–(2.5 5) | 20.68 | 0.000 |
| | (7.5 10)–(2.5 5) | 9.85 | 0.000 |
| | (7.5 15)–(2.5 5) | –0.05 | 1.000 |
| | (2.5 15)–(2.5 10) | –17.53 | 0.000 |
| | (5.0 5)–(2.5 10) | 20.82 | 0.000 |
| | (5.0 10)–(2.5 10) | 16.14 | 0.000 |
| | (5.0 15)–(2.5 10) | 17.76 | 0.000 |
| | (7.5 5)–(2.5 10) | 37.05 | 0.000 |
| | (7.5 10)–(2.5 10) | 26.22 | 0.000 |
| | (7.5 15)–(2.5 10) | 16.32 | 0.000 |
| | (5.0 5)–(2.5 15) | 38.35 | 0.000 |
| | (5.0 10)–(2.5 15) | 33.67 | 0.000 |
| | (5.0 15)–(2.5 15) | 35.29 | 0.000 |
| | (7.5 5)–(2.5 15) | 54.58 | 0.000 |
| | (7.5 10)–(2.5 15) | 43.75 | 0.000 |
| | (7.5 15)–(2.5 15) | 33.85 | 0.000 |
| | (5.0 10)–(5.0 5) | –4.68 | 0.005 |
| | (5.0 15)–(5.0 5) | –3.06 | 0.115 |
| | (7.5 5)–(5.0 5) | 16.23 | 0.000 |
| | (7.5 10)–(5.0 5) | 5.4 | 0.001 |
| | (7.5 15)–(5.0 5) | –4.5 | 0.007 |
| | (5.0 15)–(5.0 10) | 1.62 | 0.783 |
| | (7.5 5)–(5.0 10) | 20.91 | 0.000 |
| | (7.5 10)–(5.0 10) | 10.08 | 0.000 |
| | (7.5 15)–(5.0 10) | 0.18 | 1.000 |
| | (7.5 5)–(5.0 15) | 19.29 | 0.000 |
| | (7.5 10)–(5.0 15) | 8.46 | 0.000 |
| | (7.5 15)–(5.0 15) | –1.44 | 0.869 |
| | (7.5 10)–(7.5 5) | –10.83 | 0.000 |
| | (7.5 15)–(7.5 5) | –20.73 | 0.000 |
| | (7.5 15)–(7.5 10) | –9.9 | 0.000 |

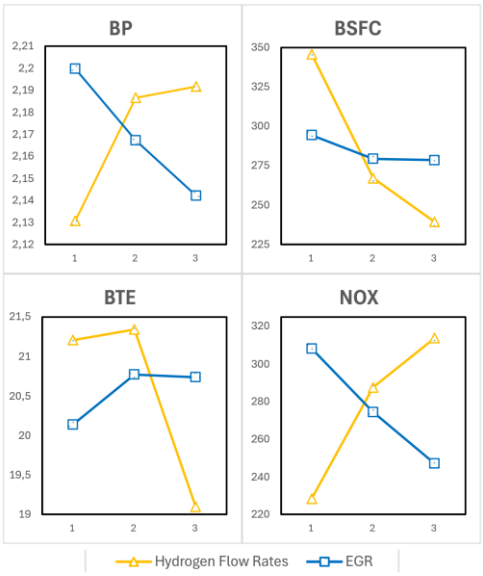


Fig. 4. Main effects plot for BP, BSFC, BTE and $NO_x$

high calorific value and rapid combustion. However, improvements in BP and BTE exhibited diminishing returns at higher flow rates. The 7.5 LPM configuration did not provide statistically significant power gains compared to 5.0 LPM ($P > 0.05$) and even reduced thermal efficiency due to lower volumetric efficiency. Therefore, the injection range of 2.5–5.0 LPM was identified as the most thermodynamically efficient operating zone.

– A clear trade–off exists between performance and emissions. Hydrogen significantly increased $NO_x$ emissions via the Zeldovich mechanism, driven by elevated combustion temperatures. While EGR effectively suppressed $NO_x$ emissions, but imposed significant penalties on engine power. Variance analysis confirmed that the interaction between these two variables was highly significant ($P \leq 0.003$). indicating that the negative impact of one variable could be mitigated by the other.
– A key statistical finding was the pattern of compensation between hydrogen and EGR. In these test conditions, hydrogen reactivity offset the power loss from EGR, simultaneously. EGR's thermal capacity reduced the $NO_x$ emission spike caused by hydrogen. Specifically, 5.0 LPM hydrogen with 10% EGR and 7.5 LPM hydrogen with 15% EGR restored $NO_x$ emissions to baseline levels ($P = 1.000$) in this engine setup.
– Considering the balance between maximum thermal efficiency fuel economy and emission compliance, the configuration of 5.0 LPM hydrogen combined with 10% EGR is recommended as the optimal operating point (Clean High–Performance). This configuration offers significant performance improvements over mono-fuel B100 mode without compromising the $NO_x$ emission profile.

**Acknowledgements**

The author would like to express sincere gratitude to the Laboratory of Thermal Engineering and Energy Systems. Institut Teknologi Sepuluh Nopember (ITS). for providing the facilities. technical support and academic environment that made this research possible. Special appreciation is extended to the supervisors and research staff whose guidance and constructive feedback greatly contributed to the completion of this work.

The author also acknowledges the valuable collaboration and encouragement from colleagues and research partners within the laboratory, whose insights and discussions enriched the study. Finally, heartfelt thanks are given to the Institut Teknologi Sepuluh Nopember for its continuous commitment to advancing research and innovation in sustainable energy systems.

## Nomenclature

| | |
|---|---|
| BP | brake power |
| BSFC | brake specific fuel consumption |
| BTE | brake thermal efficiency |
| CI | compression ignition |
| CO | carbon monoxide |
| $CO_2$ | carbon dioxide |
| EGR | exhaust gas recirculation |
| HC | hydrocarbons |
| $NO_x$ | nitrogen oxide |
| NZE | net zero emissions |
| PM | particulate matter |

## Bibliography

[1] Chicco D, Sichenze A, Jurman G. A simple guide to the use of Student's t–test. Mann–Whitney U test. Chi–squared test. and Kruskal–Wallis test in biostatistics. BioData Mining. 2025;18(1):56. https://doi.org/10.1186/s13040-025-00465-6

[2] Crippa M, Guizzardi D, Pagani F, Banja M, Muntean M, Schaaf E et al. CHG emissions of all world countries. Ispra; 2024. https://doi.org/10.2760/0115360

[3] Elnajjar EJ, Al-Omari SAB, Selim MYE, Purayil STP. CI engine performance and emissions with waste cooking oil biodiesel boosted with hydrogen supplement under different load and engine parameters. Alexandria Eng J. 2021;61(6): 4793-4805. https://doi.org/10.1016/j.aej.2021.10.039

[4] Emerson RW. ANOVA assumptions. J Vis Impair Blind. 2022;116(4):585-586. https://doi.org/10.1177/0145482X221124187

[5] European Parliament and the Council of the European Union. Regulation (EC) No 595/2009 on type–approval of motor vehicles and engines with respect to emissions from heavy duty vehicles (Euro VI). L 188; 2009.

[6] Eyal A, Thawko A, Baibikov V, Tartakovsky L. Performance and pollutant emission of the reforming–controlled compression ignition engine – experimental study. Energy Convers Manage. 2021;237:114126. https://doi.org/10.1016/j.enconman.2021.114126

[7] Krishnan MG, Rajkumar S, Devarajan Y, Rajiv A. A comprehensive review on advancement and challenges of renewable biofueled RCCI engine. J Energy Inst. 2024;113: 101540. https://doi.org/10.1016/j.joei.2024.101540

[8] Grab-Rogaliński KA, Tutak W, Jamrozik A, Kociszewski A. Comparative analysis of IC diesel engine performance

fueled with diesel/hydrogen and diesel/ammonia mixtures. Combust Engines. 2026;204(1):176-183. https://doi.org/10.19206/CE–211069

[9] Gültekin N, Gülcan HE, Ciniviz M. Investigation of the effects of hydrogen energy ratio and valve lift amount on performance and emissions in a hydrogen–diesel dual–fuel compression ignition engine. Int J Hydrogen Energ. 2024; 49:352-366. https://doi.org/10.1016/j.ijhydene.2023.07.294

[10] Indonesia Fuel Cell and Hydrogen Energy. Badan Riset dan Inovasi Nasional. Indonesia hidrogen roadmap. Bogor: IF-HE Press; 2023.

[11] Bora JB, Sharma P, Deepanraj B, Ağbulut Ü. Investigations on a novel fuel water hyacinth biodiesel and hydrogen–powered engine in dual–fuel model: optimization with I–optimal design and desirability. Fuel. 2023;345:128057. https://doi.org/10.1016/j.fuel.2023.128057

[12] Kalair A, Abas N, Saleem MS, Kalair AR, Khan N. Role of energy storage systems in energy transition from fossil fuels to renewables. Energy Storage. 2021;3(1). https://doi.org/10.1002/est2.135

[13] Kannappan C, Sengottaiyan S, Ramasamy R. The combined effect of EGR and hydrogen addition on a Syzygium cumini (Jamun) liquid biofuel engine. Biotechnol Biofuels Bioprod. 2023;16(1):1-10. https://doi.org/10.1186/s13068-023-02330-2

[14] Karagöz Y, Güler İ, Sandalcı T, Yüksek L, Dalkılıç AS. Effect of hydrogen enrichment on combustion characteristics. emissions and performance of a diesel engine. Int J Hydrogen Energ. 2016;41(1):656-665. https://doi.org/10.1016/j.ijhydene.2015.09.064

[15] Kobayashi H, Muto D, Daimon Y, Umemura Y, Takesaki Y, Maru Y et al. Experimental study on cryo–compressed hydrogen ignition and flame. Int J Hydrogen Energ. 2020; 45(7):5098-5109. https://doi.org/10.1016/j.ijhydene.2019.12.091

[16] Sagari JK, Bhatti SK, Vadapalli S, Dadi V, Guddanti SS, Lakkoju SK. Comprehensive performance. combustion. emission. and vibration parameters assessment of diesel engine fuelled with a hybrid of niger seed oil biodiesel and hydrogen: response surface methodology approach. SN Appl Sci. 2020;2(9). https://doi.org/10.1007/s42452-020-03304-x

[17] Lata DB, Ahmad A, Prakash O, Khan MM, Chatterjee R, Hasnain SMM. Impact of exhaust gas recirculation (EGR) on the emission of the dual–fuel diesel engine with hydrogen as a secondary fuel. J Inst Eng India Ser C. 2021;102(6): 1489-1502. https://doi.org/10.1007/s40032-021-00776-7

[18] Li D, Devanesan S, Kim TP, Brindhadevi K. Enhanced combustion performance and emission reduction in diesel engines fuelled by microalgae biodiesel blends with $TiO_2$ nanoparticles and hydrogen–rich biogas. Int J Hydrogen Energ. 2025;185:151933. https://doi.org/10.1016/j.ijhydene.2025.151933

[19] Marikatti MK, Banapurmath Nagaraj RR, Yaliwal VS, Basavarajappa YH, Soudagar MEM, García Marquez FP et al. Hydrogen injection in a dual fuel engine fueled with low–pressure injection of methyl ester of Thevetia peruviana (Metp) for diesel engine maintenance application. Energies. 2020;13(21). https://doi.org/10.3390/en13215663

[20] McIlwain LJ, Leong A, Bradshaw TD, Hromiak AA, Lopykinski SJ, Condon NJ et al. Optimization of oxygen and hydrogen analysis in salts by inert gas fusion. Anal Chim Acta. 2026;1382:344824. https://doi.org/10.1016/j.aca.2025.344824

[21] Ministry of Energy and Mineral Resources of the Republic of Indonesia. Peta jalan hidrogen dan amonia nasional. Jakarta: Directorate of Various New Energy and Renewable Energy; 2025.

[22] Montgomery DC. Design and analysis of experiments. 8th ed. Hoboken: John Wiley & Sons; 2012.

[23] Mousavi SM, Lipatnikov AN. Dependence of Zel'dovich number on pressure and temperature in lean hydrogen–air mixtures. Proc Combust Inst. 2024;40(1-4):105501. https://doi.org/10.1016/j.proci.2024.105501

[24] Naik GG, Dharmadhikari HM. Methods for reducing $NO_x$ and PM emissions in compression ignition engine: a review. Mater Today Proc. 2023;72:1406-1412. https://doi.org/10.1016/j.matpr.2022.09.339

[25] Palani Y, Devarajan C, Manickam D, Thanikodi S. Performance and emission characteristics of biodiesel–blend in diesel engine: a review. Environ Eng Res. 2020;27(1): 200338. https://doi.org/10.4491/eer.2020.338

[26] Rohwer J, Han T, Shah A, Rockstroh T. Investigations into EGR dilution tolerance in a pre–chamber ignited GDI engine. Int J Engine Res. 2023;24(3):1200-1222. https://doi.org/10.1177/14680874221084777

[27] Sathyamurthy R. Performance and emission characteristics of fish oil methyl ester in direct injection diesel engine with hydrogen enrichment – an experimental approach. Results Eng. 2025;26. https://doi.org/10.1016/j.rineng.2025.104983

[28] Shabana S, Sarojini J, Rao PUM, Sanijya G, Nandipati S, Barik D et al. Effect of green hydrogen enrichment and carbon nanotubes introduced biodiesel–diesel blend on the behavior of the diesel engine modified to operate on a dual–fuel mode. Energy Sci Eng. 2025;13(11):5587-5604. https://doi.org/10.1002/ese3.70268

[29] Shadidi B, Najafi G, Yusaf T. A review of hydrogen as a fuel in internal combustion engines. Energies. 2021;14(19): 6209. https://doi.org/10.3390/en14196209

[30] Skobiej K. A review of hydrogen combustion and its impact on engine performance and emissions. Combust Engines. 2025;200(1):64-70. https://doi.org/10.19206/CE-195470

[31] Vellaiyan S. Optimization of hydrogen–enriched biodiesel–diesel dual–fuel combustion with EGR for sustainable engine performance. Int J Hydrogen Energ. 2025;128:85-94. https://doi.org/10.1016/j.ijhydene.2025.04.239

[32] Winangun K, Winardi Y, Puspitasari I, Akhmad NS. Reducing exhaust emissions from palm oil biodiesel diesel engines. Automot Experiences. 2024;7(3):502-512. https://doi.org/10.31603/ae.12404

[33] Yue Z, Liu H. Advanced research on internal combustion engines and engine fuels. Energies. 2023;16(16):5940. https://doi.org/10.3390/en16165940

[34] Zhang Z, Liu H, Li Y, Ye Y, Tian J, Li J et al. Research and optimization of hydrogen addition and EGR on the combustion. performance. and emission of the biodiesel–hydrogen dual–fuel engine with different loads based on the RSM. Heliyon. 2024;10:e23389. https://doi.org/10.1016/j.heliyon.2023.e23389

Mochammad Hildad Ajiban. S.Pd. – Mechanical Engineering, Institut Teknologi Sepuluh Nopember, Indonesia.
e–mail: *6007251004@student.its.ac.id*

Prof. Dr. Ir. Bambang Sudarmanta, S.T., M.T., IPM, ASEAN. Eng. – Mechanical Engineering, Institut Teknologi Sepuluh Nopember, Indonesia.
e–mail: *sudarmanta@me.its.ac.id*